Research Article | Vol. 8, No. 8 | 1 Aug 2018 | OPTICAL MATERIALS EXPRESS 2355
Optical Materials EXPRESS

Enhancing sensing sensitivity in $Gd_2(MoO_4)_3$: Yb^{3+}/Er^{3+} upconversion phosphors by optimizing the calcination temperature

WEIJIANG XU,[1] HAOYUE HAO,[1] DONGYU LI,[2] XIAOYAN YAN,[1] YINGLIN SONG,[1] YUXIAO WANG,[1,3] AND XUERU ZHANG[1,4]

[1]*Department of Physics, Harbin Institute of Technology, Harbin 150001, China*
[2]*School of Physics Science & Technology, Lingnan Normal University, Zhanjiang 524048, China*
[3]*wangyx@hit.edu.cn*
[4]*xrzhang@hit.edu.cn*

Abstract: The X-ray diffraction result of $Gd_2(MoO_4)_3$: Yb^{3+}/Er^{3+} phosphors reveals the phase transition process associated with the calcination temperature. Under the same excitation power, the sample prepared at 700 °C shows maximal emission intensity due to the asymmetric structure of the phosphors. In addition, the optical temperature sensing behavior of the samples calcined at different calcination temperatures is also studied in detail. The maximum of absolute sensitivity is found to be 0.02533 K^{-1} at 482 K, which is obtained for the sample calcined at 700 °C. The result indicates that the samples have a great potential in optical temperature sensing.

OCIS codes: (190.7220) Upconversion; (160.2540) Fluorescent and luminescent materials; (160.4670) Optical materials; (160.5690) Rare-earth-doped materials.

References and links

1. H. Dong, L. D. Sun, and C. H. Yan, "Energy transfer in lanthanide upconversion studies for extended optical applications," Chem. Soc. Rev. **44**(6), 1608–1634 (2015).
2. J. Y. Park, K. S. Shim, and H. K. Yang, "Synthesis and photoluminescence properties of $CaGd_2(MoO_4)_4:Eu^{3+}$ red phosphors," Ceram. Int. **42**(5), 5737–5742 (2016).
3. D. M. Liu, X. X. Xu, F. Wang, J. J. Zhou, C. Mi, L. X. Zhang, Y. Q. Lu, C. S. Ma, E. Goldys, J. Lin, and D. Y. Jin, "Emission stability and reversibility of upconversion nanocrystals," J. Mater. Chem. C Mater. Opt. Electron. Devices **4**(39), 9227–9234 (2016).
4. L. M. Jin, X. Chen, C. K. Siu, F. Wang, and S. F. Yu, "Enhancing multiphoton upconversion from $NaYF_4$:Yb/Tm@$NaYF_4$ Core-Shell Nanoparticles via the Use of laser cavity," ACS Nano **11**(1), 843–849 (2017).
5. A. A. Ansari and M. Alam, "Optical and structural studies of $CaMoO_4$: Sm, $CaMoO_4$:Sm@$CaMoO_4$ and CaMoO4:Sm@CaMoO4@SiO2 core–shell nanoparticles," J. Lumin. **157**, 257–263 (2015).
6. N. Zhou, B. Xu, L. Gan, J. P. Zhang, J. B. Han, and T. Y. Zhai, "Narrowband spectrally selective near-infrared photodetector based on up-conversion nanoparticles used in a 2D hybrid device," J. Mater. Chem. C Mater. Opt. Electron. Devices **5**(7), 1591–1595 (2017).
7. Y. C. Cao, Z. Y. Zhao, J. Yi, C. S. Ma, D. C. Zhou, R. F. Wang, C. Li, and J. B. Qiu, "Luminescence properties of Sm^{3+}-doped TiO_2 nanoparticles: Synthesis, characterization, and mechanism," J. Alloys Compd. **554**, 12–20 (2013).
8. J. Liu, A. M. Kaczmarek, and R. V. Deun, "Concentration and temperature dependent upconversion luminescence of $CaWO_4$: Er^{3+}, Yb^{3+} 3D microstructure materials," J. Lumin. **188**, 604–611 (2017).
9. A. M. Khachatourian, F. G. Fard, H. Sarpoolaky, C. Vogt, E. Vasileva, M. Mensi, S. Popov, and M. S. Toprak, "Microwave synthesis of $Y_2O_3:Eu^{3+}$ nanophosphors: A study on the influence of dopant concentration and calcination temperature on structural and photoluminescence properties," J. Lumin. **169**, 1–8 (2016).
10. Z. L. Wu, B. J. Chen, X. P. Li, J. S. Sun, J. S. Zhang, H. Zhong, H. Zheng, L. L. Tong, X. Q. Zhang, and H. P. Xia, "Calcination temperature optimization, energy transfer mechanism and fluorescence temperature dependence of $KLa(MoO_4)_2:Eu^{3+}$ phosphors," J. Phys. Chem. Solids **88**, 96–103 (2016).
11. L. P. Li, L. J. Zheng, W. Xu, Z. Liang, Y. Zhou, Z. G. Zhang, and W. W. Cao, "Optical thermometry based on the red upconversion fluorescence of Er^{3+} in $CaWO_4:Yb^{3+}/Er^{3+}$ polycrystalline powder," Opt. Lett. **41**(7), 1458–1461 (2016).
12. H. Y. Hao, Z. M. Lu, H. Y. Lu, G. H. Ao, Y. L. Song, Y. X. Wang, and X. R. Zhang, "Yb^{3+} concentration on emission color, thermal sensing and optical heater behavior of Er^{3+} doped $Y_6O_5F_8$ phosphor," Ceram. Int. **43**(14), 10948–10954 (2017).

#330986 https://doi.org/10.1364/OME.8.002355
Journal © 2018 Received 4 May 2018; revised 15 Jul 2018; accepted 17 Jul 2018; published 25 Jul 2018

Optical Materials EXPRESS

13. A. Pandey, V. K. Rai, V. Kumar, V. J. Kumar, and H. C. Swart, "Upconversion based temperature sensing ability of Er^{3+}–Yb^{3+} codoped $SrWO_4$: An optical heating phosphor," Sens. Actuators B Chem. **209**, 352–358 (2015).
14. D. Q. Chen, M. Xu, and P. Huang, "Core@shell upconverting nanoarchitectures for luminescent sensing of temperature," Sens. Actuators B Chem. **231**, 576–583 (2016).
15. W. B. Bi, Q. Y. Meng, W. J. Sun, and S. C. Lu, "Optical temperature sensing properties of Er^{3+}, Yb^{3+} co-doped $NaGd(MoO_4)_2$ phosphor," Ceram. Int. **43**(1), 1460–1465 (2017).
16. M. Mondal, V. K. Rai, and C. Srivastava, "Influence of silica surface coating on optical properties of Er^{3+} - Yb^{3+}:$YMoO_4$ upconverting nanoparticles," Chem. Eng. J. **327**, 838–848 (2017).
17. T. T. Yan, D. S. Zhang, L. Y. Shi, H. P. Yang, H. L. Mai, and J. H. Fang, "Reflux synthesis, formation mechanism, and photoluminescence performance of monodisperse Y_2O_3:Eu^{3+} nanospheres," Mater. Chem. Phys. **117**(1), 234–243 (2009).
18. D. Zhao, F. X. Ma, P. G. Duan, C. K. Nie, J. F. Guo, and R. J. Zhang, "Commensurately modulated structure and luminescent properties of $Na_3Pr(PO_4)_2$," J. Lumin. **192**, 129–135 (2017).
19. Y. N. Bao, X. S. Xu, J. L. Wu, K. C. Liu, Z. Y. Zhang, B. S. Cao, and B. Dong, "Thermal-induced local phase transfer on Ln^{3+} -doped $NaYF_4$ nanoparticles in electrospun ZnO nanofibers: Enhanced upconversion luminescence for temperature sensing," Ceram. Int. **42**(10), 12525–12530 (2016).
20. Z. Huang, Z. Q. Nie, M. B. Xie, Y. X. Wang, and D. Y. Li, "Excellent optical thermometry based on upconversion emission in $SrMoO_4$:Er^{3+} phosphor," Opt. Mater. Express **7**(7), 2404 (2017).
21. X. F. Wang, Q. Liu, Y. Y. Bu, C. S. Liu, T. Liu, and X. H. Yan, "Optical temperature sensing of rare-earth ion doped phosphors," RSC Advances **5**(105), 86219–86236 (2015).
22. M. Quintanilla, I. X. Cantarelli, M. Pedroni, A. Speghini, and F. Vetrone, "Intense ultraviolet upconversion in water dispersible SrF_2:Tm^{3+}, Yb^{3+} nanoparticles: the effect of the environment on light emissions," J. Mater. Chem. C Mater. Opt. Electron. Devices **3**(13), 3108–3113 (2015).
23. S. Sinha, M. K. Mahata, K. Kumar, S. P. Tiwari, and V. K. Rai, "Dualistic temperature sensing in Er^{3+}/Yb^{3+} doped $CaMoO_4$ upconversion phosphor," Spectrochim. Acta A Mol. Biomol. Spectrosc. **173**, 369–375 (2017).
24. H. Y. Lu, R. Meng, H. Y. Hao, Y. F. Bi, Y. C. Gao, Y. L. Song, Y. X. Wang, and X. R. Zhang, "Stark sublevels of Er^{3+}–Yb^{3+} codoped $Gd_2(WO_4)_3$ phosphor for enhancing the sensitivity of a luminescent thermometer," RSC Advances **6**(62), 57667–57671 (2016).
25. X. Chai, J. Li, X. S. Wang, Y. X. Li, and X. Yao, "Color-tunable upconversion photoluminescence and highly performed optical temperature sensing in Er^{3+}/Yb^{3+} co-doped $ZnWO_4$," Opt. Express **24**(20), 22438–22447 (2016).
26. P. Du, L. H. Luo, Q. Y. Yue, and W. P. Li, "The simultaneous realization of high- and low-temperature thermometry in Er^{3+}/Yb^{3+}-codoped Y_2O_3 nanoparticles," Mater. Lett. **143**, 209–211 (2015).
27. A. K. Soni, A. Kumari, and V. K. Rai, "Optical investigation in shuttle like BaMoO4:Er^{3+}–Yb^{3+} phosphor in display and temperature sensing," Sens. Actuators B Chem. **216**, 64–71 (2015).
28. B. Dong, D. P. Liu, X. J. Wang, T. Yang, S. M. Miao, and C. R. Li, "Optical thermometry through infrared excited green upconversion emissions in Er^{3+}–Yb^{3+} codoped Al_2O_3," Appl. Phys. Lett. **90**(18), 181117 (2007).
29. W. Xu, Z. Zhang, and W. Cao, "Excellent optical thermometry based on short-wavelength upconversion emissions in Er^{3+}/Yb^{3+} codoped $CaWO_4$," Opt. Lett. **37**(23), 4865–4867 (2012).
30. M. Quintanilla, E. Cantelar, F. Cusso, M. Villegas, and A. C. Caballero, "Temperature Sensing with Up-Converting Submicron-Sized $LiNbO_3$:Er^{3+}/Yb^{3+} Particles," Appl. Phys. Express **4**(2), 022601 (2011).
31. L. Mukhopadhyay and V. K. Rai, "Upconversion based near white light emission, intrinsic optical bistability and temperature sensing in Er^{3+}/Tm^{3+}/Yb^{3+}/Li^{+}:$NaZnPO_4$ phosphors," New J. Chem. **41**(15), 7650–7661 (2017).
32. M. K. Mahata, K. Kumar, and V. K. Rai, "Er^{3+}-Yb^{3+} doped vanadate nanocrystals: A highly sensitive thermographic phosphor and its optical nanoheater behavior," Sens. Actuators B Chem. **209**, 775–780 (2015).
33. N. Rakov and G. S. Maciel, "Three-photon upconversion and optical thermometry characterization of Er^{3+}:Yb^{3+} co-doped yttrium silicate powders," Sens. Actuators B Chem. **164**(1), 96–100 (2012).

1. Introduction

It is reported that upconversion (UC) materials have excellent chemical stability, strong and stable luminescence properties, long luminescence lifetimes [1,2] and so on, which accounts for their popularity in materials chemistry research. In recent years, UC materials had many excellent properties, which were applied to various fields such as multi-modal imaging, magnetic resonance imaging, information security, solar-energy harvesting and conversion [3–6], etc.

It is well known that various factors have significant influence on the morphology, crystalline phase and luminescence properties of a material, such as the use of different ligands, PH, reaction temperature and reaction time [7,8]. Adrine et al. reported that Y_2O_3: Eu^{3+} nano-phosphor was prepared by a microwave method as the calcination temperature increased from 700 to 1050 °C. The luminescence intensity of the peaks increased proportionally with the increase of the calcination temperature as a result of improved

Optical Materials EXPRESS

crystallinity, growth in the crystallite size and removal of organic groups [9]. However, the influence of the calcination temperature on the crystalline phase and luminescence properties on $Gd_2(MoO_4)_3$: Yb^{3+}/Er^{3+} (GMO: Yb^{3+}/Er^{3+}) particles has been much less investigated. If the calcination temperature is too low, the starting materials will not completely react; In contrast, if the calcination temperature is too high, the particles will aggregate together at least and more than that the starting materials will melt to form bulk ceramic [10]. Therefore, exploring optimum calcination temperature is one of the aims of this work.

Unlike traditional measurement of temperature relying on the principle of heat-expansion and cold-contraction, optical temperature sensing has unique advantages, such as noncontact [11], fast response, anti-electromagnetic interference, and so on. In general, the temperature can be measured through probing the temperature-dependent fluorescence intensity ratio (FIR) of two thermal coupled levels (TCL), whose energy gap ranges from 200 to 2000 cm^{-1} [12,13]. The TCL $^2H_{11/2}$ and $^4S_{3/2}$ of Er^{3+} ions have been used widely in optical temperature sensing due to their larger energy gap, intense green emissions and minor overlap between two green emission peaks. It is expected that the high sensing sensitivity can be achieved in Yb^{3+}/Er^{3+} co-doped materials for the practical applications. To realize the goal, some parameters including host matrix, doping concentration and luminescence intensity were studied previously [14,15]. Chen et al. studied the effect of shell thickness on temperature sensing. Compared to the core-only nanoparticles, thermal effect induced by the irradiation of 980 nm laser of the core@shell particles could be neglected, which benefited for obtaining intense FIR signal and detecting temperature accurately [14]. However, the effect of calcination temperature on optical temperature sensing always has been ignored.

In the calcination temperature range from 600 to 900 °C, GMO: Yb^{3+}/Er^{3+} crystals are successfully prepared via a sol-gel method. The influence of the calcination temperature on the crystal structure is investigated by means of X-ray diffraction (XRD). The luminescence properties of the crystals are analyzed by fluorescence spectroscopy. The optimal calcination temperature is experimentally achieved. The properties of fluorescence influenced by the calcination temperature are studied in details. Furthermore, the optical temperature sensing behavior of the samples annealed at different calcination temperatures is also researched.

2. Experimental

2.1. Sample preparation

The Yb^{3+} and Er^{3+} co-doped GMO crystals are synthesized using a sol-gel method. Based on the previous work and literature, the ratio of Yb^{3+} to Er^{3+} ions is chosen to be 9:1. Firstly, 0.9 mmol $Yb(NO_3)_3.6H_2O$, 0.1 mmol $Er(NO_3)_3.6H_2O$, 9 mmol $Gd(NO_3)_3.6H_2O$, 15 mmol $(NH_4)_6Mo_7O_{24}.4H_2O$ are dissolved in 50 ml distilled water and the citric acid as chelating agent is added to this solution. The concentration ratio of citric acid and metal ions used in this experiment is 1:1.5. And then, the pH of the solution is adjusted to 7 by adding appropriate ammonia. The mixture heats at 80 °C under continuous magnetic stirring for 30 minutes. After that, the wet gel is dried at 130 °C for 20 h. Subsequently, the mixtures are transferred to the alumina crucibles followed by the calcination in a furnace at temperature from 600 to 900 °C for 2 h in air atmosphere with a heating rate of 10 °C/min. Finally, these mixtures are cooled down to room temperature naturally.

2.2. Characterization

The XRD pattern is recorded on an X-ray diffractometer (Empyrean, Panalytical, Netherlands) at a scanning rate of 4°min^{-1} in the 2θ range from 10° to 50° with Cu-Ka radiation (= 0.15406 nm). The luminescence spectrum collected from the sample is recorded by using a Spectrometer (HORIBA Jobin Yvom iHR550) in the wavelength range of 500-700 nm. A 980 nm diode laser (Bejing Kipling Photoelectric technology Co., Ltd.) is used to be the excitation source. For the thermometry experiments, a heating stage (Linkam THMS 600)

Optical Materials EXPRESS

is employed to heat the sample, and the temperature is measured by the thermocouple. The Scanning Electron Microscopy (SEM) images are achieved using a Quanta 200FEG-SEM with a working voltage of 30 kV.

3. Results and discussion

3.1. Structural characterization

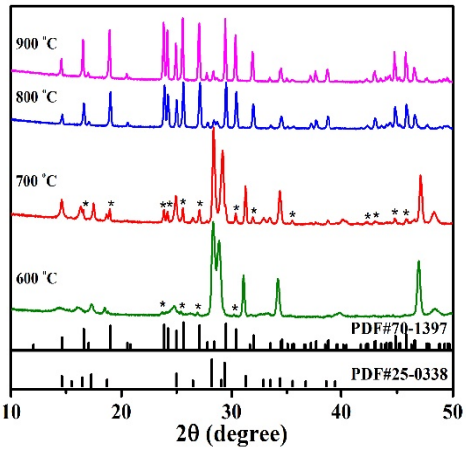

Fig. 1. XRD patterns of GMO: Yb^{3+}/Er^{3+} phosphors prepared at different calcination temperature (* represents orthorhombic).

In order to study the effect of calcination temperature on the crystalline structure of Yb^{3+}/Er^{3+} co-doped GMO powders, XRD measurement is carried out. The XRD pattern of Yb^{3+}/Er^{3+} co-doped GMO powders annealed from 600 to 900 °C for 2 h is shown in Fig. 1. The XRD pattern of the sample synthesized at 600 °C is similar to that of the sample annealed at 700 °C. Their XRD patterns show that most of crystalline phases are monoclinic phase (PDF#25-0338) and a few are orthorhombic crystal (PDF#70-1397). When calcination temperature reaches to 800 °C, the orthorhombic phase completely appears and no diffraction peaks can be detected, indicating that the Yb^{3+} and Er^{3+} ions have been effectively built into the GMO host lattice. From Fig. 1, it can be seen that the samples synthesized at a temperature higher than 700 °C exhibit pure GMO with standard orthorhombic phase (PDF#70-1397).

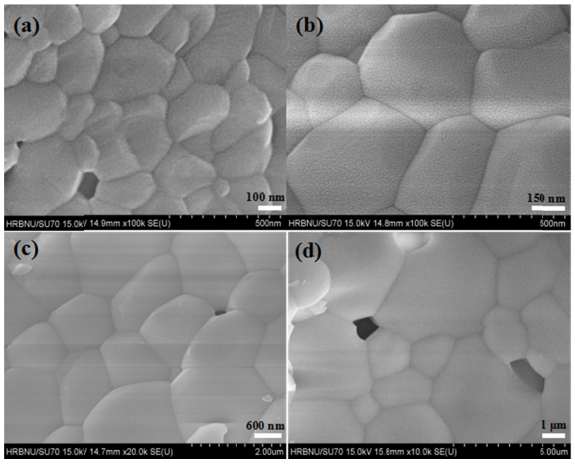

Fig. 2. SEM images of GMO: Yb^{3+}/Er^{3+} crystals sintered at different temperatures. (a) 600 °C, (b) 700 °C, (c) 800 °C, (d) 900 °C.

Optical Materials EXPRESS

Figure 2 shows the SEM images GMO: Yb^{3+}/Er^{3+} crystals corresponding to different calcination temperatures. From Fig. 2 (a)-(d), particles are aggregated together rather than dispersed and the samples have irregularly surface morphology as the calcination temperature rises from 600 to 900 °C. Furthermore, as the calcination temperature rose from 600 to 900 °C, the minimum size and maximum size of the GMO: Yb^{3+}/Er^{3+} samples increase gradually from 50 to 1000 nm and rise gradually from 150 to 3000 nm, respectively. It indicates that the calcination temperature has an important influence on the particle size of GMO: Yb^{3+}/Er^{3+} phosphors.

3.2. Upconversion emission study

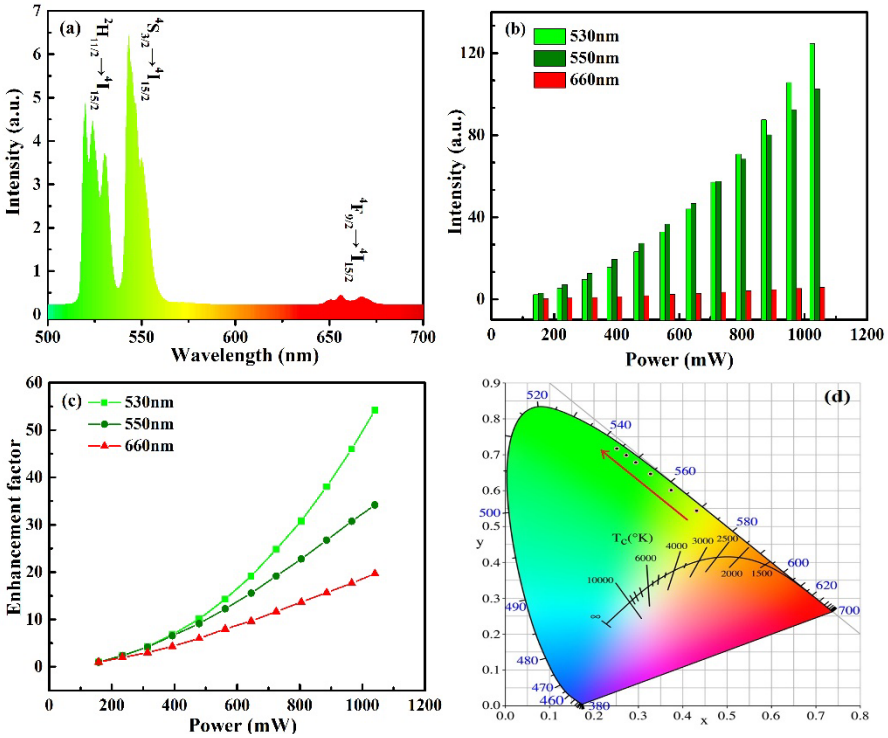

Fig. 3. (a) PL spectra of GMO: Yb^{3+}/Er^{3+} phosphors annealed at 800°C under 980 nm excitation, (b) Power dependence of green and red emissions, (c) corresponding enhancement factor of green and red emissions as a function of excitation powers, (d) CIE chromaticity diagram of GMO: Yb^{3+}/Er^{3+} phosphors at different excitation powers.

The emission spectra of GMO:Yb^{3+}/Er^{3+} phosphors excited by a 980 nm laser is shown in Fig. 3(a), revealing remarkably intense green and relatively weak red emissions. Three emission peaks located around 530 nm、550 nm and 660 nm could be assigned to the $^2H_{11/2} \rightarrow {}^4I_{15/2}$, $^4S_{3/2} \rightarrow {}^4I_{15/2}$ and $^4F_{9/2} \rightarrow {}^4I_{15/2}$ transitions of Er^{3+} ions, respectively. From Fig. 3(b), an obvious increase in PL intensity is found for green emission bands over the excitation powers range from 158 to 1040 mW, while luminescent intensity of red mission bands shows a slight enhancement. As shown in Fig. 3(c), it is noteworthy that PL enhancement factors are different for various emission bands. The PL intensities of the 530, 550 and 660 nm emission bands at 1040 mW pump power are approximately 54, 34 and 20 times higher than those at 158 mW, respectively. Yb^{3+} ions have higher absorption cross section at 980 nm to provide efficient energy transfer rate as a sensitizer [31]. As the power increases, Yb^{3+} ions can absorb more photons and transport them to corresponding excited states through energy transfer. Therefore, PL intensity of the sample will increase with enhancing the power. The colour

Optical Materials EXPRESS

coordinates are calculated at different pump powers in the Commission Internationale de I'Eclairage (CIE) chromaticity diagram as shown in Fig. 3(d). The colour coordinates are found to be varied from yellow-green region towards the pure green region when increasing the excitation power from 158 mW (0.43, 0.54) to 1040 mW (0.25,0.72), indicating that the pumper power can regulate and control color.

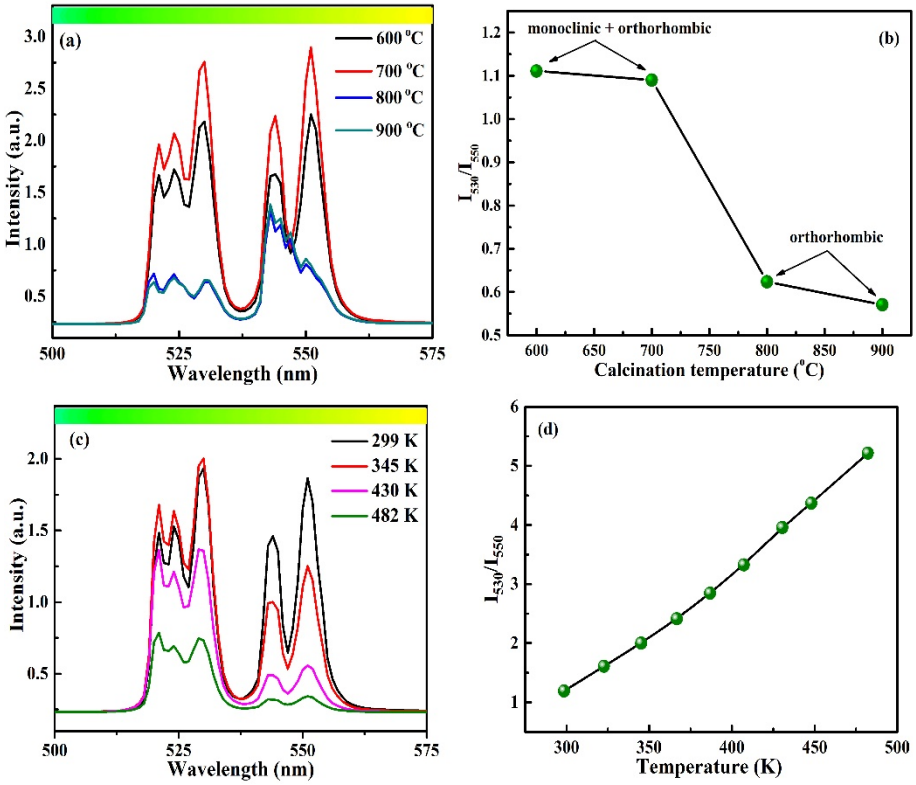

Fig. 4. (a) Luminescence spectra of GMO: Yb^{3+}/Er^{3+} phosphors annealed at temperature from 600 to 900 °C under 253 mW power excitation of a 980 nm laser, (b) The green at 530 nm -to-green at 550 nm emission intensity ratio (I_{530}/I_{550}) at various calcination temperatures, (c) Emission spectra of GMO: Yb^{3+}/Er^{3+} crystal annealed at 700°C as a function of absolute temperature under 176 mW pump power excitation, (d) I_{530}/I_{550} as a function of temperature from 299 K to 482 K.

Green emission bands play a key role in our study. Hence we only select 500-575 nm as our research object. To explore the effect of different calcination temperatures on luminescence properties, we measure photoluminescence spectra at room temperature. With increasing the calcination temperature, the luminescence intensities for all peaks increase. But the calcination temperature further increases to 800 °C, the emission intensities start to decrease, which can be seen from Fig. 4(a). Moreover, the sample prepared at 700 °C shows maximal emission intensity. These phenomena can be explained by the facts as follows. On the one hand, as the calcination temperature increases, surface defect reduces and the crystallinity increases [16–18], thus luminescence intensity increases. On the other hand, compared with orthorhombic phase, monoclinic phase has better asymmetry. It is well known that asymmetric phase structure is more conducive to the enhancement of fluorescence [19]. Asymmetric phase structure has lower symmetry, which contributes to the enhancement of crystal field. The rare-earth ions in a crystal field with lower symmetry are susceptible to be excited. Therefore, the emission intensities decrease rapidly from 700 to 800 °C. As shown in Fig. 4(a), when the calcination temperature is above 800 °C, the fluorescent intensities on

Optical Materials EXPRESS

emission band at 530 and 550 nm have little change with increasing the calcination temperature. It may be due to a fact that the size of the sample annealed at 900 °C is too large.

As shown in Fig. 4(b), the transition $^2H_{11/2}\rightarrow{}^4I_{15/2}$ (the green emission at 530 nm) is more dominant than the transition $^4S_{3/2}\rightarrow{}^4I_{15/2}$ (the green emission at 550 nm) from 600 to 700 °C, while from 800 to 900 °C the $^4S_{3/2}\rightarrow{}^4I_{15/2}$ transition is more dominant. Figure 4(c) shows the green emission spectra of GMO: Yb^{3+}/Er^{3+} crystals at different temperatures under the excitation of a 980 nm laser, and all the emission peaks do not shift as temperature rises. From Fig. 4(c), I_{530} increases gradually with increasing temperature from 299 K to 345 K, then it decreases continuously with increasing temperature from 345 K to 482 K. These results can be attributed to the competition between the thermal agitation and non-radiative relaxation of $^2H_{11/2}$ level [20,21]. Besides, I_{550} significantly decreases as temperature from 299 K rises to 482 K. According to the multi-phonon non-radiative decay rate

$$W_m(T) = W_0(0)[1-\exp(-\frac{h\nu}{kT})]^{-m} \quad (1)$$

where $W_0(0)$ and $W_m(T)$ are the multi-phonon non-radiative decay rate at temperature 0 K and T K, respectively. $m = \Delta E/h\nu$ is the number of phonons and ΔE is the energy gap between the two states involved. $h\nu$ is the phonon energy of the matrix. T is the absolute temperature, and k is Boltzmann's constant. As T rises, $W_m(T)$ increases. Hence, the thermal effect can lead to the quenching of the emission [22]. It can be seen that the I_{530}/I_{550} continuously increases with increasing temperature in Fig. 4(d), which is opposite to the one in Fig. 4(b).

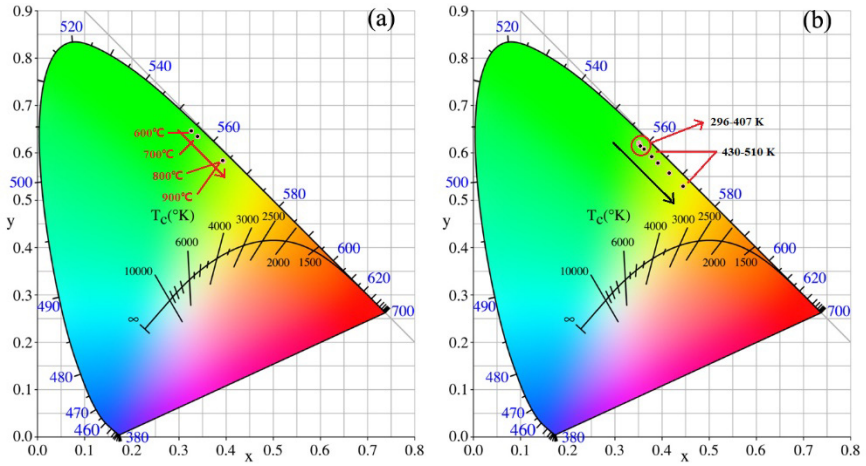

Fig. 5. (a) CIE coordinate diagram of GMO: Yb^{3+}/Er^{3+} phosphors annealed at different temperatures under 253 mW power excitation of a 980 nm laser, (b) Color coordinates of GMO: Yb^{3+}/Er^{3+} crystal annealed at 700°C at various temperatures under 176 mW excitation..

CIE coordinate diagram of GMO: Yb^{3+}/Er^{3+} phosphors annealed at different temperatures is showed in Fig. 5(a). It can be found that the color coordinates move from green to yellow region as the calcination temperature rises. Figure 5(b) shows the CIE chromaticity diagram of GMO: Yb^{3+}/Er^{3+} crystals upon 980 nm excitation. The color coordinates were calculated at different temperature. It is observed that the color coordinates move towards the more yellow region with increasing temperature.

3.3. Temperature sensing study

In order to investigate the influence of the calcination temperature on the temperature sensing behavior in GMO:Yb^{3+}/Er^{3+} phosphors, the green emissions located around 530 nm and 550 nm are recorded at the temperature range of 299-510 K upon 980 nm excitation. As shown in

Optical Materials EXPRESS

Fig. 6(a), the I_{530}/I_{550} of samples annealed at different calcination temperature increases as temperature rises.

The populations in two states are ruled by Boltzmann distribution. Therefore, the *FIR* can be given as follows

$$FIR = \frac{I_{530}}{I_{550}} = \mathrm{C}\exp\left(-\frac{\Delta \mathrm{E}}{kT}\right) \tag{2}$$

where C is the pre-exponential constant, ΔE is the energy difference between the $^2H_{11/2}$ and $^4S_{3/2}$ levels, k is Boltzmann's constant and T is absolute temperature. Then Eq. (2) can be converted in the form of a linear equation as

$$\mathrm{Ln}(FIR) = \mathrm{Ln}\,\mathrm{C} + \left(-\frac{\Delta \mathrm{E}}{kT}\right) \tag{3}$$

According to Eq. (3), absolute sensitivity (S_a) is defined as

$$S_a = \frac{\mathrm{d}R}{\mathrm{d}T} = R\left(\frac{\Delta \mathrm{E}}{kT^2}\right) \tag{4}$$

Substituting the different values of Ln(R) and 1/T into Eq. (3), the ΔE/k and LnC values can be obtained by linear fitting. As shown in Fig. 6(b), the logarithm of Ln(R) linearly fits well with the inverse of T. The fitted linear functions are as follows

$$\mathrm{Ln}(R_1) = 4.0 - \frac{1159.15}{T} \tag{5}$$

$$\mathrm{Ln}(R_2) = 4.0 - \frac{1134.85}{T} \tag{6}$$

$$\mathrm{Ln}(R_3) = 3.5 - \frac{1208.06}{T} \tag{7}$$

$$\mathrm{Ln}(R_4) = 3.5 - \frac{1187.52}{T} \tag{8}$$

where R_1, R_2, R_3 and R_4 are the fluorescence intensity ratio (I_{530}/I_{550}) of 600, 700, 800 and 900 °C, respectively. In order to know the thermometry's capacity of the samples, we calculate absolute sensitivity by Eq. (4), and the results are as follows

$$S_{a1} = \frac{63289.59}{T^2}\exp\left(-\frac{1159.15}{T}\right) \tag{9}$$

$$S_{a2} = \frac{61962.81}{T^2}\exp\left(-\frac{1134.85}{T}\right) \tag{10}$$

$$S_{a3} = \frac{40010.95}{T^2}\exp\left(-\frac{1208.06}{T}\right) \tag{11}$$

$$S_{a4} = \frac{39330.66}{T^2}\exp\left(-\frac{1187.52}{T}\right) \tag{12}$$

where S_{a1}, S_{a2}, S_{a3} and S_{a4} are the absolute sensitivity of 600, 700, 800 and 900 °C, respectively. The S of samples calcined at different calcination temperatures are shown in Fig.

Optical Materials EXPRESS

6(c). It can be found that the maximum value for the S_a of the sample calcined at 600, 700, 800, 900 °C is 0.02436, 0.02533, 0.01311 and 0.01344 K^{-1}, respectively.

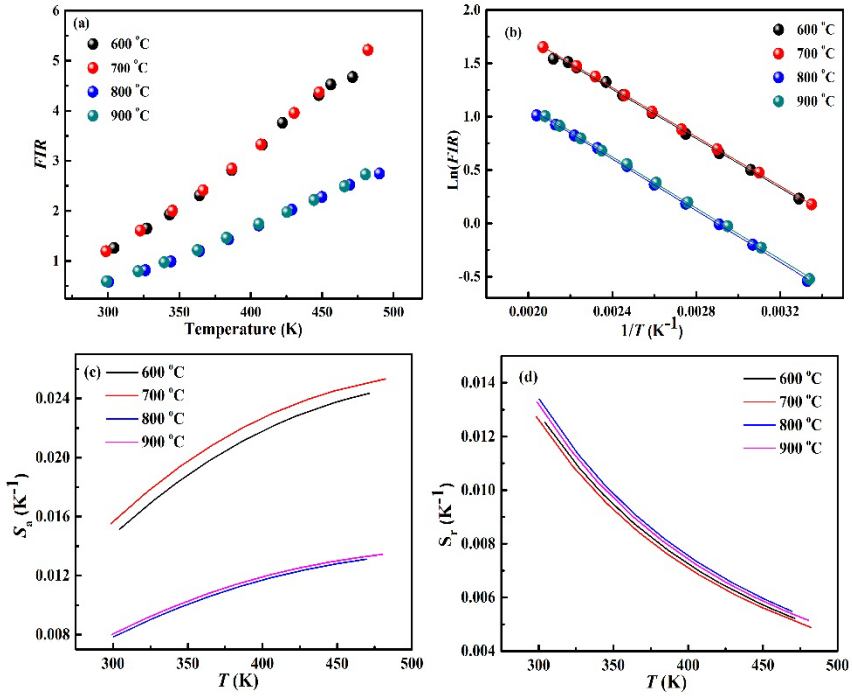

Fig. 6. (a) The *FIR* variation of different samples as a function of temperature upon 176 mW power excitation, (b) The value of Ln(*R*) dependence on 1/*T* in GMO: Yb^{3+}/Er^{3+} phosphors at different calcination temperature, (c) The absolute sensitivities (S_a) of GMO: Yb^{3+}/Er^{3+} crystals prepared at 600, 700, 800 and 900 °C, (d) The relative sensitivities (S_r) of GMO: Yb^{3+}/Er^{3+} crystals sintered at different temperatures as a function of temperature.

When the calcination temperature is 700 °C, a maximal sensitivity of 0.02533 K^{-1} at 482 K can be achieved, which is quite different from that of the samples annealed at 800 and 900 °C. Furthermore, the temperature sensing properties of the sample calcined at 600 °C is similar to that of the sample annealed at 700 °C, while the sample calcined at 800 °C has similar temperature sensing behavior with the sample calcined at 900 °C. It is well known that the *R* is one of the most important parameters to estimate optical temperature sensitivity ($S_a = R\Delta E/kT^2$). It may attribute to a fact that the local field of Er^{3+} ions is modified with the phase transition and the probability of the downward radiation transition in the excitation states corresponding to the two luminescence peaks is changed, leading to the variation of I_{530}/I_{550} (FI*R*). Therefore the S_a of the samples calcined at 600 and 700 °C are obviously greater than that of the samples calcined at 800 and 900 °C.

Relative sensitivity (S_r) can be defined as

$$S_r = \frac{1}{R}\frac{dFIR}{dT} = \frac{\Delta E}{kT^2} \tag{13}$$

From Eq. (13), ΔE plays a key role in S_r. As shown in Fig. 6(d), the S_r of sample calcined at different temperature continually decreases with the increase of temperature. The comparison of temperature sensing properties in Yb^{3+}/Er^{3+} co-doped various oxide host matrices applying FIR technique is shown in Table 1. Compared with some other Yb^{3+}/Er^{3+} co-doped oxide materials for optical temperature sensing, although the S_r of the GMO: Yb^{3+}/Er^{3+} phosphors annealed at 700 °C is not the greatest, the S_a of the sample has been improved a lot, indicating

Optical Materials EXPRESS

that the GMO: Yb^{3+}/Er^{3+} phosphors are promising materials for applications in optical temperature sensing.

Table 1. The comparison of temperature sensing properties of Yb^{3+}/Er^{3+} co-doped oxide materials.

Materials	Excitation wavelength (nm)	Max. S_a (K^{-1})	S_r (K^{-1})	Temperature range (K)	Ref.
$CaMoO_4$	980	0.0072	$1072/T^2$	535-760	[23]
$NaGd(MoO_4)_2$	980	0.0161	$969.7/T^2$	298-593	[15]
$SrWO_4$	980	0.01498	$866.05/T^2$	300-518	[13]
$02YMoO_4@SiO_2$	980	0.024	$1274.46/T^2$	301-368	[16]
$Gd_2(WO_4)_3$	980	0.0165	$1790/T^2$	296-620	[24]
$ZnWO_4$	980	0.0099	$1134.937/T^2$	83-583	[25]
Y_2O_3	980	0.0044	$886.08/T^2$	93-613	[26]
$BaMoO_4$	980	0.0206	$873.38/T^2$	303-523	[27]
Al_2O_3	978	0.0051	$964.1/T^2$	295-973	[28]
$CaWO_4$	980	0.0073	$2109.31/T^2$	303-873	[29]
$LiNbO_3$	980	0.0075	$1250/T^2$	285-453	[30]
GMO:Yb^{3+}/Er^{3+} (600 °C)	980	0.02436	$1159.15/T^2$	299-482	This work
GMO:Yb^{3+}/Er^{3+} (700 °C)	980	0.02533	$1134.85/T^2$	299-482	This work
GMO:Yb^{3+}/Er^{3+} (800 °C)	980	0.01311	$1208.06/T^2$	299-482	This work
GMO:Yb^{3+}/Er^{3+} (900 °C)	980	0.01344	$1187.52/T^2$	299-482	This work

To assess accuracies of the S_a and S_r, the error δ is researched. The error δ between $\triangle E_f$ and $\triangle E_e$ is expressed by the following equation [21]

$$\delta = \frac{\left|\Delta E_f - \Delta E_e\right|}{\Delta E_e} \tag{14}$$

where $\triangle E_f$ is the fitting value of $\triangle E$, and $\triangle E_e$ is experimental value calculated from the two green emission peaks in the spectrum. $\triangle E_e$ is obtained from the spectra in Fig. 4 (a). The error δ is a key parameter to determine whether the value of $\triangle E_f$ agrees well with the experiment value of $\triangle E_e$ [21].

Table 2. The comparison of $\triangle E_f$, $\triangle E_e$ and δ of Yb^{3+}/Er^{3+} co-doped phosphors.

Materials	$\triangle E_f$ (cm^{-1})	$\triangle E_e$ (cm^{-1})	δ (%)	Ref.
YVO_4:Yb^{3+}/Er^{3+}	538	693	22.36	[32]
$CaWO_4$:Yb^{3+}/Er^{3+}	1455	1530	4.90	[13]
Al_2O_3:Yb^{3+}/Er^{3+}	679.4	771.8	11.97	[28]
Y_2SiO_3:Yb^{3+}/Er^{3+}	781	686.1	13.83	[33]
$SrWO_4$:Yb^{3+}/Er^{3+}	602	766.1	21.42	[29]
$BaMoO_4$:Yb^{3+}/Er^{3+}	607	716	15.22	[26]
$LiNbO_3$:Yb^{3+}/Er^{3+}	860	686.2	25.33	[30]
Y_2O_3:Yb^{3+}/Er^{3+}	615.7	800	23.0	[27]
GMO:Yb^{3+}/Er^{3+} (600 °C)	805.6	686.1	18.16	This work
GMO:Yb^{3+}/Er^{3+} (700 °C)	788.7	686.1	14.95	This work
GMO:Yb^{3+}/Er^{3+} (800 °C)	839.6	686.1	22.37	This work
GMO:Yb^{3+}/Er^{3+} (900 °C)	825.3	686.1	20.29	This work

By using Eq. (14), the errors δ of the samples prepared at 600 °C, 700 °C, 800 °C and 900 °C are calculated to be 18.16%, 14.95%, 22.37% and 20.29%, respectively. It is more than 10%, which is attributed to a fact that the energy transfer between the host and the rare-earth ions cannot be ignored [21]. The comparisons of $\triangle E_f$, $\triangle E_e$ and δ of Yb^{3+}/Er^{3+} co-doped phosphors are shown in Table 2.

Optical Materials EXPRESS

4. Summary

In summary, $Gd_2(MoO_4)_3$:Yb^{3+}/Er^{3+} phosphors with various crystalline phases are synthesized by changing the annealing temperature via a sol-gel method. The XRD result of the sample reveals that the phase transformation completely occurs with increasing the calcination temperature. When the calcination temperature reaches to 800 °C, the impurity phase absolutely transforms into the orthorhombic phase. In addition, the sample prepared at 700 °C shows maximal emission intensity under 980nm excitation, mainly attributed to a fact that monoclinic phase which has better asymmetry structure is more beneficial to the enhancement of fluorescence compared with orthorhombic phase. Moreover, the maximum sensitivity is found to be 0.02533 K^{-1} at 482 K obtained for the sample calcined at 700 °C due to the variation of *FIR* caused by phase transition, suggesting that the $Gd_2(MoO_4)_3$:Yb^{3+}/Er^{3+} phosphors are promising materials for applications in optical temperature sensing.

Funding

National Natural Science Foundation of China (Grant Nos. 11474078 and 11404283). Natural Science Foundation of Guangdong Province (Grant No. 2014A030307028).